Available online at www.sciencedirect.com
ScienceDirect
International Journal of Thermal Sciences 46 (2007) 506–518
International Journal of Thermal Sciences
www.elsevier.com/locate/ijts

Turbulent heat transfer and pressure drop in tube fitted with serrated twisted tape

Shyy Woei Chang [a,*], Yih Jena Jan [b], Jin Shuen Liou [a]

[a] *Thermal Fluids Laboratory, Department of Marine Engineering, National Kaohsiung Marine University, No. 142, Haijhuan Rd., Nanzih District, Kaohsiung, Post Code: 811, Taiwan, ROC*

[b] *Department of Marine Engineering, National Kaohsiung Marine University, No. 142, Haijhuan Rd., Nanzih District, Kaohsiung, Post Code: 811, Taiwan, ROC*

Received 15 November 2005; received in revised form 12 July 2006; accepted 12 July 2006

Available online 22 August 2006

Abstract

This paper presents an original experimental study on compound heat transfer enhancement in a tube fitted with serrated twisted tape. The serrations on two sides of the twisted tape with twist ratio of 1.56, 1.88, 2.81 or ∞ are the square-sectioned ribs with the identical rib-pitch and rib-height. The local Nusselt number and Fanning friction factor increase as the twist ratio decreases in the tube fitted with smooth or serrated twisted tape. In the *Re* range of 5000–25 000, heat transfer augmentation attributed to the serrated twisted tape falls in the range of 250–480% of the plain-tube level. That is about 1.25–1.67 times the heat transfer level in the tube fitted with smooth twisted tape. Fanning friction factors are respectively decreased and increased in the tubes fitted with smooth and serrated twisted tapes as *Re* increases. Based on the same pumping power consumption, the thermal performances of the tubes with smooth and serrated twisted tapes are compared. A set of empirical correlations that permits the evaluation of the Nusselt number and the Fanning friction factor in the developed flow region for the tubes fitted with smooth and serrated twisted tapes is generated for engineering applications.

Keywords: Twisted tape with serrations mean Nusselt numbers; Mean fanning friction coefficients

1. Introduction

Passive heat transfer-enhancement (HTE) techniques, such as the use of wavy, roughened and extended surfaces and the insertion of swirl generator, are implemented with the expense of additional energy consumption due to the increased pressure drop. The twisted tape insert generates considerable HTE with a reasonable increase in pressure drop that is often applied to the design of tubular heat exchangers and to the improvement of thermal performance in existing heat transfer equipment. The swirling flow generated by a continuous twisted tape in a tube persists over the entire duct length that modifies the vorticity distribution in the flow core. The formation of continuous swirling flow and the modification of near wall velocity profile due to the various vorticity distributions in the vortex core are concluded as two major factors for HTE in swirl pipes [1].

HTE in a duct fitted with twisted tape is additionally generated by the partitioning and blockage of ducted flow, the fin effect of metallic insert and the elongated twisted flow path [2–10]. In turbulent flow regime, the pair of swirling streams is characterized by rather uniform axial velocity in a form of vortexes that exist in any cross-section of a tube with twisted tape insert [2]. With heating conditions of uniform heat-flux and uniform wall-temperature, Hong and Bergles [3] reported the heat transfer correlation for fully developed flow. In Manglik and Bergles [4,5] the laminar flow and turbulent flow of HTE in a tube with twisted tape insert was defined. For this class of HTE measures, Reynolds number (*Re*) and twist ratio (y) are the two main controlling parameters signifying the friction and heat transfer characteristics in a duct with twisted tape insert.

It is a general trend that HTE in a tube with a twisted tape insert falls dramatically in the transition and turbulent flow regimes; but increases with the increase of y [8]. Heat transfer in a tube with twisted tape insert could be respectively raised up to 30 and 3.5 times of the plain tube level for lam-

* Corresponding author.
E-mail address: swchang@mail.nkmu.edu.tw (S.W. Chang).

1290-0729/$ – see front matter
doi:10.1016/j.ijthermalsci.2006.07.009

Nomenclature

C_p	specific heat at constant pressure	$\mathrm{J\,kg^{-1}\,K^{-1}}$	
d	diameter of the smooth tube	m	
e	rib height	m	
f	Fanning friction factor, $= \frac{\Delta P}{0.5\rho W_m^2}(\frac{d}{4L})$		
$\bar{f}$	Fanning friction factor for developed flow		
f_∞	Fanning friction factor for developed flow in smooth walled plain tube		
k_f	thermal conductivity of fluid	$\mathrm{W\,m^{-1}\,K^{-1}}$	
L	length between two pressure tappings	m	
n	exponent of Reynolds number in Nusselt number correlation		
Nu	local Nusselt number, $= \frac{q_f d}{(T_w - T_f)k_f}$		
$\overline{Nu}$	spatially averaged Nusselt number for developed flow		
Nu_∞	Nusselt number value for developed flow in smooth walled plain tube		
P	axial distance of twist pitch with 180° rotation of tape	m	
P_R	rib pitch	m	
Pr	Prandtl number of coolant ($\mu C_p/k_f$)		
ΔP	pressure difference between two pressure taps	$\mathrm{N\,m^{-2}}$	
q_f	convective heat flux	$\mathrm{W\,m^{-2}}$	
Re	Reynolds number, $= \frac{\rho W_m d}{\mu}$		
T_f	fluid bulk temperature	K	
T_w	wall temperature	K	
W_m	mean flow velocity	$\mathrm{m\,s^{-1}}$	
x	axial location referred to flow entry as origin	m	
X	dimensionless axial location (x/d)		
y	twist ratio (P/d)		

Greek symbols

α	rib angle of attack	degree
ρ	density of fluid	$\mathrm{kg\,m^{-3}}$
μ	fluid dynamic viscosity	$\mathrm{kg\,m^{-1}\,s^{-1}}$
η	performance factor, $= (\overline{Nu}/Nu_\infty)/(\bar{f}/f_\infty)^{1/3}$	

Abbreviation

SR	serration roughened
SW	smooth walled

inar ($Re < 2000$) and turbulent ($5000 < Re < 45\,000$) flows [11]. The twisted tape insertion was accordingly treated as an effective HTE measure for laminar flow but to be less effective for augmenting turbulent flow heat transfer. Recently, Sarma et al. [12] derived the generalized correlations to evaluate friction factors (f) and the Nusselt number (Nu) in a tube with twisted tape insert using the experimental data mining from the open literature. Justified by the data trends revealed in [12], they inferred that the presence of a twisted tape inhibited the transitional jump from laminar to turbulent flow in view of f vs. Re relationship, which led to the monotonic laminar to turbulent transition. The different Nu and f enhancement ratios between the laminar and turbulent flows in a tube with twisted tape insert, as reported in [8,11], are caused by the different plain-tube Nu and f references selected for laminar and turbulent flows.

Further improvements of thermal performance for a duct with twisted tape insert are continued when attempting to use the regularly spaced twisted tape elements [13,14], the combination of spirally corrugated tubes with a continuous twisted tape [15,16], the twisted tape insert in a square duct [17,18] and the insertion of multiple twisted tapes in a tube [19,20]. The research goals [13–20] involve the further increase of HTE ratio and thermal performance factor with the extended effective Re range. In a tube fitted with regularly spaced twisted tape elements connected by a circular rod, the pressure drop could be reduced by up to 40% of that found in the tube with full-length twisted tape insert without impairing its heat transfer rate [13,14]. Accordingly, the thermal performance factor for the tube fitted with regularly spaced twisted tape elements is improved [13,14]. Several combinations of two or more HTE measures that generate higher heat transfer rates compared to those obtained with the single HTE measure include the use of twisted tape [15,16,21,22]. The insertion of continuous twisted tape in a corrugated tube could increase the heat transfer coefficients to 1.9–9.6 times of the plain tube value in the Re range of 3000–60 000 [15]. The insertion of a combined swirl-generator that consists of the internal twisted tape with the external tape to be spirally wound on the internal tape [22] could provide higher HTE ratios than those generated in tubes with single twisted tape insert. This type of enhanced twisted tape [22] not only offered an HTE ratio comparable with that generated in a corrugated tube fitted with twisted tape [16] but also considerably extended the effective Re range for HTE. Nevertheless, the retrofit applications for upgrading the HTE performances of existing heat transfer equipment are limited for this class of compound HTE measures [15,16,22] due to the need to change the existing tubes in heat exchangers. With consideration to retrofit applications, the twisted tape insert in a square (rectangular) duct was initially studied [17,18]. In a square duct fitted with a continuous twisted tape, the swirling flow was subject to the periodical weakness at the gaps between the twisted tape and the duct wall so that the spatially periodical heat transfer profile was established [17]. Relative to the circular tube with a continuous twisted tape insert, the periodically weakened swirl in a square duct fitted with twisted tape resulted in a less HTE ratio for laminar flow. But the periodical bursting swirls developed in the clearances between the twisted tape and the duct wall, which modified the near wall flow structures, could extend the effective Re range for HTE. Heat transfer coefficients in a square duct fitted with the continuous twisted tape were increased by the factors of 1.8 to 4.5 times over the plain tube levels [18]. As the bursting swirls in a square duct with a continuous twisted tape insert could extend the effective Re range for HTE [15–18], the HTE and thermal performance of a tube

fitted with multiple twisted tapes were examined [19]. In a tube with multiple twisted tape inserts, both HTE ratio and effective *Re* range increase with the increase in the number of twisted tapes. In the *Re* range of 3000–14 000, the tubes fitted with twin and triple twisted tapes could offer the higher HTE ratios with similar levels of thermal performance factors as those found in the tube fitted with single twisted tape. The HTE effect in a tube fitted with multiple twisted tapes may be amplified if the HTE performance attributed from each single twisted tape can be further improved. This triggered the present study to investigate the heat transfer and pressure drop in the tube fitted with a continuous twisted tape with serration. In a duct with two opposite walls roughened by repeated surface ribs, the rib-induced secondary flows accompanied by enhanced turbulence intensity and the boundary layer redevelopments provide considerable HTE impacts. The present study develops another type of compound HTE measure using serration-roughened (SR) twisted tape inserts in a tube. The characteristics of heat transfer, pressure drop and thermal performance factor in the tubes fitted with smooth walled (SW) and SR twisted tapes of different twist ratios are compared. The correlations of Nusselt number (Nu) and Fanning friction factor (f) for the developed flow in SW and SR tubes are derived to assist with industrial applications.

2. Experimental details

The test section for heat transfer and pressure drop measurements is depicted in Fig. 1(a). The twisted tapes with and without serrations having the twist ratios (y) of 1.56, 1.88, 2.81 and ∞ are shown in Fig. 1(b). The pressure drop tests were separately performed from the heat transfer tests using the isothermal flows.

As shown in Fig. 1(a), the test tube (1) containing a continuous serrated twisted tape is made from a seamless stainless' steel tube with a bore diameter of 15 mm, a wall thickness of 3 mm and a nominal length of 300 mm. Each twisted tape (2) with and without serrations has identical width and thickness of 15 and 1.5 mm, respectively. The twisted tape with serrations is made from straight tape with two sides roughened by repeated ribs as shown as the twisted tape with $y = \infty$ in Fig. 1(b). The rib height (e), rib pitch (P_R) and rib angle-of-attack (α) are defined by the straight tape with serrations in Fig. 1(b). The test conditions with the straight twisted tape insert in the tube are approximated as the test conditions with $y = \infty$. The measurements of heat transfer and pressure drop in the tube with straight tape provide the necessary limiting base line references for the present HTE problem.

These repeated surface ribs are attached on both sides of the twisted tape with serrations that have the identical set of geometric parameters of:

- Rib angle of attack (α) = 90° (identified from the straight twisted tape with $y = \infty$);
- Rib height (e) to diameter of smooth tube (d) ratio = 1.5 (mm)/15 (mm) = 0.1;
- Rib pitch (P_R) to rib height (e) ratio = 15 (mm)/1.5 (mm) = 10.

Two insulating bushes (3) and (4) hold the plenum chamber (5) and the test tube (1) by four draw bolts (6) to give a heated length of 290 mm between the end bush and plenum chamber. The ratio of cross sectional areas between the plenum chamber and the test-tube is referred to as the abrupt ratio of flow-entrance is 2. A pair of twin start threads having the same pitch of 3 mm but different depth is machined onto the outer surface of test tube (1) to install the wall thermocouples (7) and the electrical heating wire (8). The deeper thread is used for embedding 39 equally spaced K type thermocouples (7) along the radial outer edge of test tube. Axial locations of these 39 thermocouples are indicated in Fig. 1(a). The depth of this deep thread is selected to keep the sensing junction of each thermocouple 0.4 mm away from the inner bore of test tube. The Ni/Ch alloy resistance wire (8) is spirally wound into the 1 mm pitched thread machined on the outer surface of the test tube to supply the heating power. Depth of the groove for heating wire is 1.25 mm.

The external heat loss from heat transfer test tube prohibits all the supplied heating power to be convected by the flow. The local convective heat flux is obtained by subtracting the heat loss flux from the total heat flux generated by heating wire. The amount of external heat loss increases with the increase of wall-to-ambient temperature difference. A non-uniform wall temperature distribution over the tube surface generates the non-uniform heat loss flux distribution. As the total heat flux is uniformly supplied by the electrical heating wire, the uniformity of convective heat flux is determined by the non-uniform distribution of heat loss flux. With the adequate thermal insulation for the test section, the maximum amount of external heat loss is about 5.44% of total heat supplied after reviewing all the heat flux data generated for three sets of heat transfer tests. Basically uniform heat flux heating condition is confirmed.

The characteristic of heat loss is determined based on the results of heat loss calibration runs. To perform the heat loss calibration tests, the flow passage is blocked and filled with wool. The supplied heat flux from the heating wire is balanced with the external heat loss flux when the wall-to-ambient temperature difference remains fixed. The proportionality between the external heat loss flux and the wall-to-ambient temperature difference is obtained, which is incorporated into the program of data processing to evaluate the local heat loss flux.

Coolant leakage from the contacting surfaces between the constructional parts of each test section is prevented by means of a series of internal O ring seals. Two additional thermocouples (9) and (10) penetrate the core of the plenum–chamber and the passage in the exit bush (4) to measure the flow entry and exit temperatures, respectively. A Teflon tube (11) is used to stiffen the final assembly. In order to minimize the external heat loss during the heat transfer experiments, the outer surface of the stiffening tube (11) is wrapped with the thermal insulation material.

Seven, ten or twelve probing tubes were equipped with pressure taps of 0.5 mm diameter at the locations corresponding to

(1-a) Construction details of the heat transfer test module

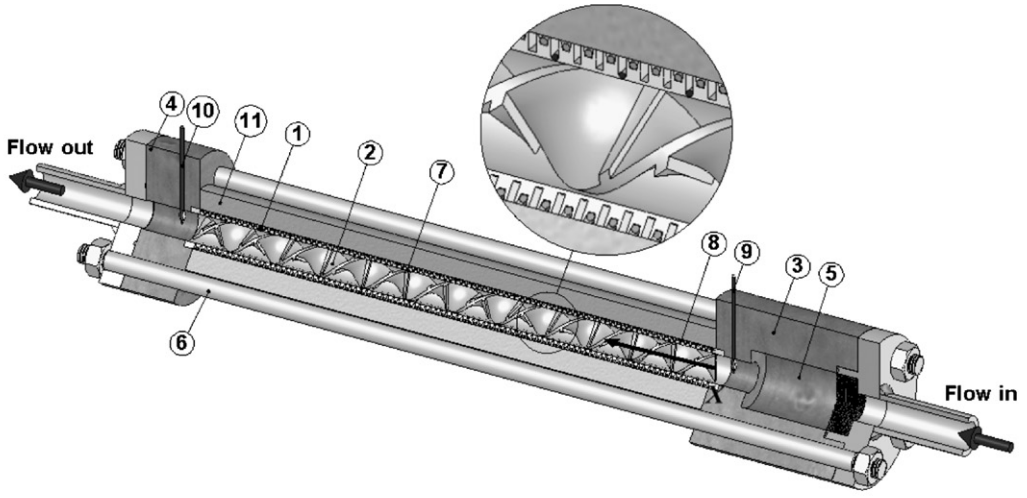

(1) Test tube
(2) Twisted tape
(3) Entry insulating bush
(4) Exit insulating bush
(5) Plenum chamber
(6) Draw bolt
(7) Thermocouple measuring wall temperature
(8) Heating wire
(9) Thermocouple measuring flow entry temperature
(10) Thermocouple measuring flow exit temperature
(11) Teflon stiffing tube

(1-b) Rib roughened and smooth walled twisted tapes

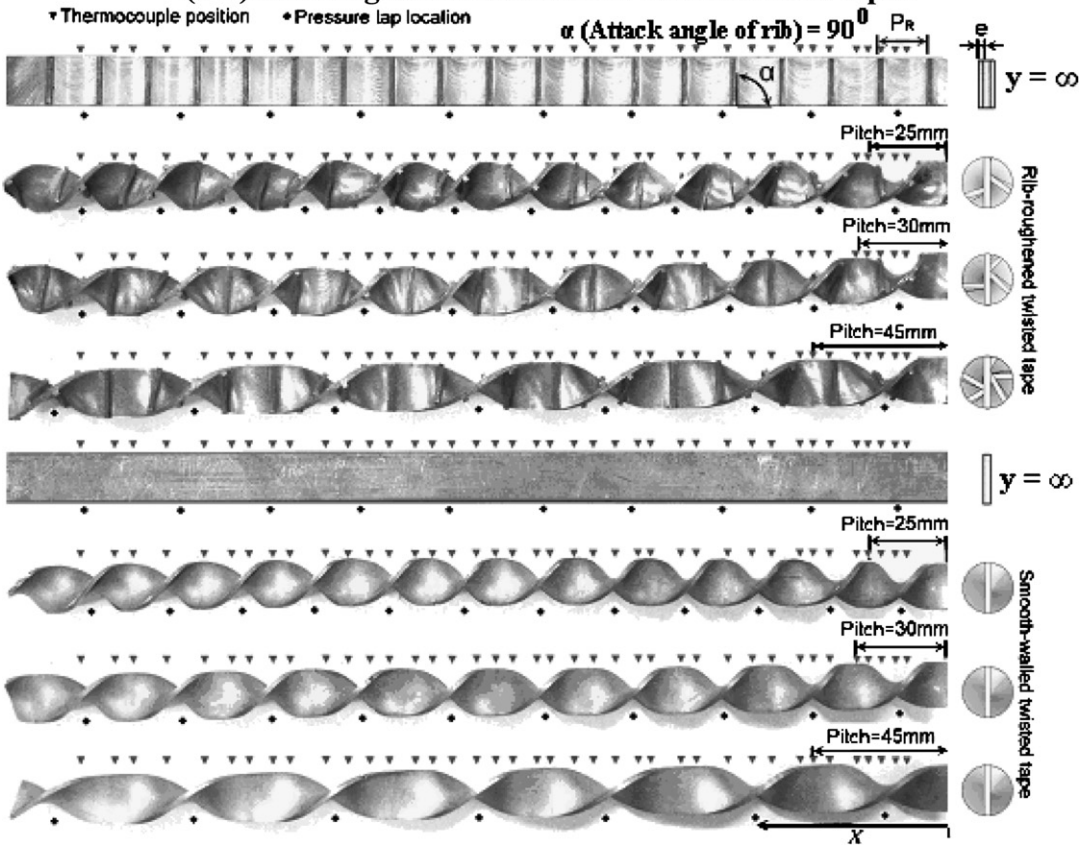

Fig. 1. Experimental apparatus.

the mid-pitches of the twisted tape as indicated in Fig. 1(b) to measure the pressure drops along the test tubes with twisted tape inserts of $y = 1.56$, 1.88 and 2.81. A short 1 mm diameter stainless steel tube was glued on the top of each pressure tapping as the connection for the flexible tube. It is noted that, as the three twisted tapes with the twist ratios of 1.56, 1.88 and 2.81 have different pitches, the mid-pitch locations for these three twisted tapes correspond to different axial locations on the tubes. Therefore, three test tubes with the pressure tapings allocated at the precise mid-pitch locations for three twisted tapes of $y = 1.56$, 1.88 and 2.81 are used for the series of pressure drop measurements. The pressure difference between two taps was measured by a Rosemount digital type micro manometer. The precision of this micro manometer was 0.01 mm H_2O which provided the maximum uncertainty about 5% for this series of tests. The friction factor evaluated from the pressure difference between two pressure taps was specified at the mid-span location of these two taps, which corresponds to the pitch location of each twisted tape with twist ratios of 1.56, 1.88 and 2.81.

This experimental program, using dry air as the test coolant, involves three phases. The axial *Nu* distributions along the test tube with smooth walled (SW) or serration roughened (SR) twisted tape of four twist ratios are measured at $Re = 5000$, 10 000, 15 000, 20 000 and 25 000. The *Nu* data generated in this phase of study is compared with the Dittus–Boelter correlation level [23] to assess the HTE ratios generated by the SW and SR twisted tapes with four twist ratios. The second phase of experimental program performs the pressure drop measurements for SW and SR tubes at each targeting Reynolds number. The pressure drop tests are conducted at the isothermal conditions. The Fanning friction factors obtained at each tested Reynolds number for SW or SR tube are normalized by the Blasius equation for turbulent flow in order to unravel the pressure drop augmentations in SW or SR tube. Having acquired the heat transfer and pressure drop data, the performance factors based on the constant pump power consumption are evaluated for each test condition with insertion of SW or SR twisted tape. It is then followed by a third phase of regression type analysis to get the heat transfer and pressure drop correlations for the test tube fitted with SW or SR twisted tape.

At each targeting *Re* value, the flow and heating level are fixed for about 45 minutes in order to assure the steady state condition. When the differences between several successive wall temperature scans remain within ±0.3 K, the steady state is assumed and the on line data acquisition system is activated. This set of raw experimental data is subsequently processed into the corresponding *Re* and *Nu* data and the effect of *Re* on *Nu* distribution is examined. When the local heat flux at any location on the tube surface is quantified then by the Newton's cooling law, the local *Nu* data is experimentally defined as

$$Nu = \frac{q_f d}{(T_w - T_f)k_f} \tag{1}$$

where q_f, T_w, T_f and k_f in Eq. (1) respectively stand for convective heat flux, wall temperature at the inner core of test tube, fluid bulk temperature and thermal conductivity of coolant. The wall temperature at the inner core of the test tube is corrected from the measured wall temperature using one-dimensional Fourier conduction law.

The Fanning friction factor, f, was calculated from the pressure drop, ΔP, across two successive pressure taps with the interval length of L and the mean flow velocity W_m as:

$$f = \frac{\Delta P}{0.5\rho W_m^2}\left(\frac{d}{4L}\right) \tag{2}$$

The approximation of experimental uncertainties for the present data reduction process was conducted [24]. The temperature and pressure drop measurements were the major sources for uncertainty. With the differences in temperature and pressure drop measurements in the ranges of 40–79 K and 16–178 mm H_2O, the maximum uncertainties for *Nu*, *Re* and f were about 9.3% and 7.6% and 9.1%, respectively.

To determine the HTE ratio and the pressure drop increase in the present test tube, the comparative references of heat transfer and friction factor were selected as the levels in a smooth walled circular tube with fully developed flow. The reference Nusselt number, Nu_∞, and friction factor, f_∞, were evaluated as:

$$Nu_\infty = 0.023Re^{0.8}Pr^{1/3} \tag{3}$$

(Dittus–Boelter correlation for turbulent flow)

$$f_\infty = 0.079Re^{-0.25} \tag{4}$$

(Blasius equation for turbulent flow)

The thermal performance of the test tube with SW or SR twisted tape insert was quantified by the performance factor, η. This performance factor, η, is defined as:

$$\eta = (\overline{Nu}/Nu_\infty)/(\bar{f}/f_\infty)^{1/3} \tag{5}$$

3. Results and discussion

3.1. Heat transfer results

The axial distributions of Nusselt numbers along the SW tube with twist ratios of 1.56, 1.88, 2.81 and ∞ at Reynolds numbers of 5000, 10 000, 15 000, 20 000 and 25 000 are displayed in Figs. 2(a), 2(b), 2(c) and 2(d), respectively. Local heat transfers consistently increase with an increase in the Reynolds number as shown in Fig. 2. The cross examination of *Nu* data obtained at each targeting *Re* value with different twist ratio in Fig. 2 indicates the decrease of *Nu* level as y increases, which reflects the diminished swirling flow as the severity of the twisted tape is decreased. The relative HTE impact in SW tube with $y = \infty$ is about 1.6 times of the smooth walled plain tube level. As the cooling area ratio between the SR tube and the smooth walled plain tube is 1.55, the HTE effect in the SW tube with $y = \infty$ is mainly attributed from the fin effect of the twisted tape insert. As shown in Fig. 2, each *Re* controlled axial *Nu* variation in the SW tube demonstrates the well-known approach to the fully developed flow that occurs as the flow and thermal boundary layers are developed. The initially high Nusselt number at the entry region decays to a fully developed value after the flow travels about 6 tube-diameters downstream of the

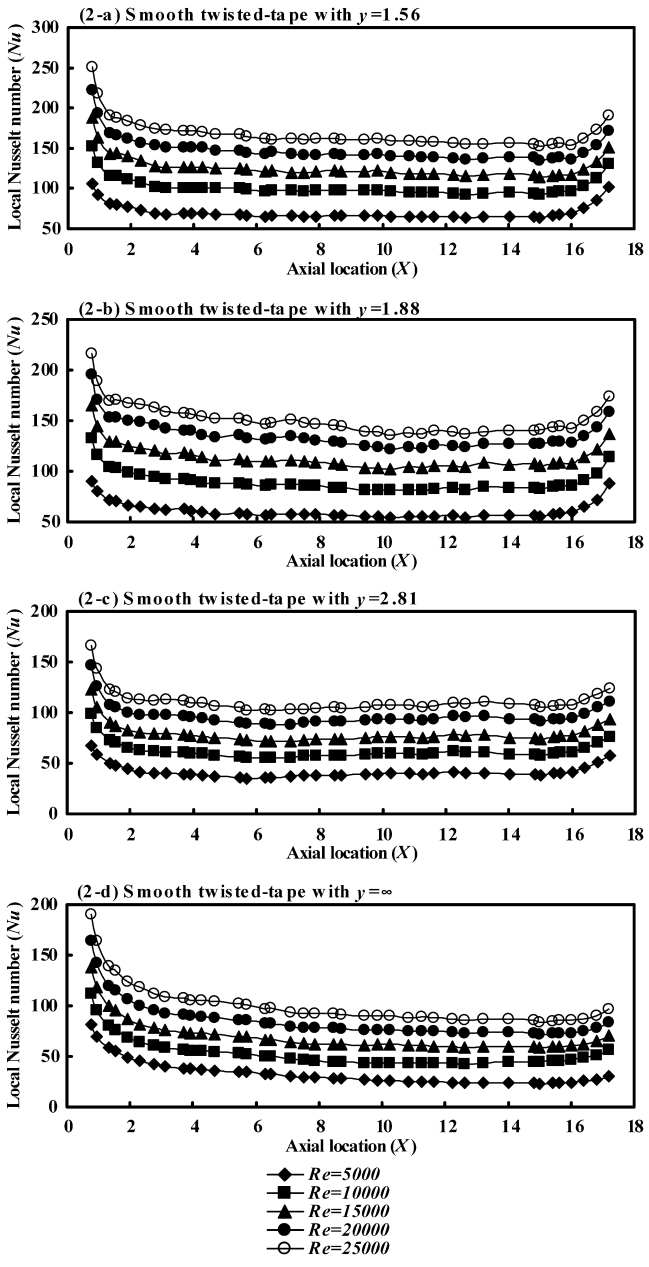

Fig. 2. Axial distributions of heat transfer in SW tube.

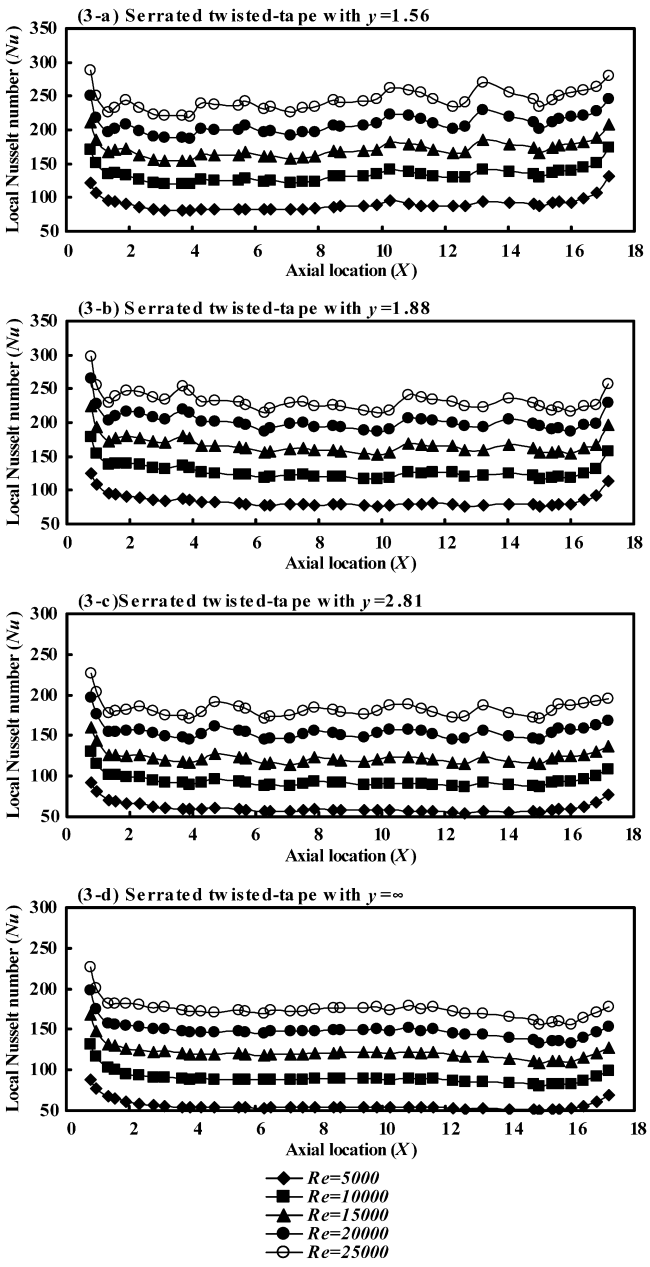

Fig. 3. Axial distributions of heat transfer in the SR tube.

flow entrance. The Nusselt number data in the final axial region of $x/d > 16$ is increased by the usual exit loss effect present in this type of experiment. Heat transfer data influenced by the exit loss effect in this final region is disregarded for subsequent data analysis. The Nusselt number results collected from all the axial stations in the developed flow region of $6 < x/d < 16$ are averaged to generate the developed flow Nusselt number in the SW tube as $\overline{Nu}_{SW}$.

Fig. 3 follows the manner of plotting Fig. 2 to determine the axial *Nu* variation in the tube fitted with serrated twisted tape. The axial locations which specify the entry and exit-loss regions in the SR tubes generally agree with those detected in the SW tubes. As the swirling flow effects diminish in the SR tube by increasing the twist ratio, the HTE effects are systematically moderated. For the limiting condition of $y = \infty$ in the SR tube, the attack angle of each surface rib on the twisted tape is 90° to the main stream direction so that the vortical flow cells remain stagnant behind each rib. The flow re-attachment and the enhanced turbulence intensity are the main flow physics for HTE. The local *Nu* data in the SR tube with $y = \infty$ is about 2.5 times of the smooth walled plain tube level. But the cooling area ratio between the SR tube and the smooth walled plain-tube is 1.67. Thus in the SR tube with $y = \infty$, the rib-induced vortical flows and the enhanced turbulence intensity play a significant role for HTE in addition to the fin effect of the straight serrated twisted tape.

Fig. 3 also depict the *Nu* versus *Re* trend showing that the local Nusselt numbers in the SR tube increase with the increase of *Re*. However, the *Re* controlled wavy like axial *Nu* distribution in the SR tube gradually emerges as *Re* increases from 5000

to 25 000. In the SR tube with a finite twist ratio, the ribs attached on the serrated twisted tape follow the surface curvature of the twisted tape. Justified by the channel flow roughened by the skewed ribs, the flow cells behind each rib on the serrated twisted tape are no longer stagnant. These vortices are swept by the twisted tape induced swirling flows and convection in a downstream direction. Because the wavy like axial *Nu* variation is not detected in the SW tube and in the SR tube with $y = \infty$, the flow interactions between the secondary flows triggered by the repeated ribs and the tape-induced swirling flows are likely to promote the generation of large scale longitudinal vortical flow structure in the twisted flow passage of the SR tube. The interactive mechanism between the serration triggered vortical cells and the swirling flows induced by the twisted tape is the dominant flow physic that provides the HTE effects in the SR tube. Nevertheless, although the wavy like *Nu* variations prevail in the SR tube at the high Reynolds numbers tested, the Nusselt number data collected from all the axial locations in the region of $6 < x/d < 16$ is averaged to represent the heat transfer level for the developed flow in the SR tube, which is referred to as $\overline{Nu}_{SR}$.

The HTE ratios generated by the SW and SR twisted tapes from the plain tube conditions are indexed as the Nusselt number ratio in terms of $\overline{Nu}_{SW,SR}/\overline{Nu}_{\infty}$ where the Nusselt number reference, Nu_{∞}, is evaluated from the Dittus–Boelter correlation [23]. In order to determine the relative heat transfer enhancement in SR tube from the SW tube condition, the HTE ratio is alternatively referred to as the relative Nusselt number defined as $\overline{Nu}_{SR}/\overline{Nu}_{SW}$. The variations of $\overline{Nu}_{SW,SR}/\overline{Nu}_{\infty}$ and $\overline{Nu}_{SR}/\overline{Nu}_{SW}$ with *Re* are plotted in Figs. 4(a) and 4(b), respectively. As a reconfirmation of the typical results found in a tube fitted with twisted tape, Fig. 4(a) demonstrates that the increase of *Re* and twist ratio (y) in either SW or SR tube systematically reduces the $\overline{Nu}_{SW,SR}/\overline{Nu}_{\infty}$ ratio. In the *Re* range of 5000–25 000, the ratios of $\overline{Nu}_{SW,SR}/\overline{Nu}_{\infty}$ obtained with four twist ratios of 1.56, 1.88, 2.81 and ∞ fall in the ranges of 3.5–2.34, 2.99–2.07, 2.12–1.59 and 1.35–1.31 for the SW tube and in the ranges of 4.8–3.68, 4.21–3.36, 3.06–2.66 and 2.84–2.53 for the SR tube. While the SR tubes still offer considerable heat transfer augmentations of about 3–4 times of plain-tube level at *Re* of 25 000. The extension of effective *Re* range for HTE using the serrated twisted tape insert is assured. To view the relative heat transfer enhancement in SR tube from the SW tube level, the variations of $\overline{Nu}_{SR}/\overline{Nu}_{SW}$ against *Re* are plotted in Fig. 4(b). In the *Re* range of 5000–25 000 with four twist ratios of 1.56, 1.88, 2.81 and ∞, the $\overline{Nu}_{SR}/\overline{Nu}_{SW}$ ratios are in the range of 1.37–2.1. This particular result confirms the further HTE derived from the interactive mechanism between the serration triggered vortical cells and the swirling flows induced by the twisted tape in the SR tube. As the value of $\overline{Nu}_{SR}/\overline{Nu}_{SW}$ consistently increases as *Re* increases for each twist ratio examined, the effectiveness of serrations for HTE in a tube with a twisted tape insert is enhanced as *Re* increases. However, when the twist ratio remains finite, the highest $\overline{Nu}_{SR}/\overline{Nu}_{SW}$ ratio develops in the tube fitted with the tape of the largest twist ratio of 2.81 y at each tested *Re*. The SR tube with twist ratio of 1.56 provides the higher $\overline{Nu}_{SR}/\overline{Nu}_{\infty}$ ratios than the counterparts of 1.88 y. In light of the

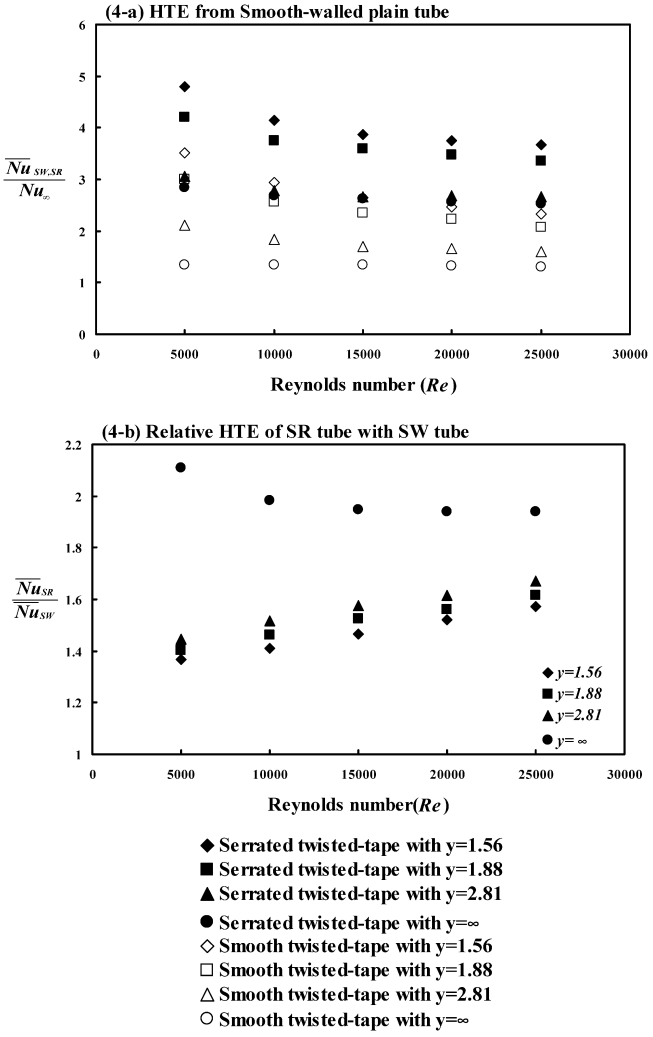

Fig. 4. Variations of Nusselt number ratios with Reynolds number in tubes fitted with twisted tape.

inconsistency between $\overline{Nu}_{SR}/\overline{Nu}_{\infty}$ and $\overline{Nu}_{SR}/\overline{Nu}_{SW}$ versus y relationships revealed in Figs. 4(a) and 4(b), there should be the optimal combinations of rib-pitch with twist-pitch that could offer the largest HTE effects in the SR tube.

While developing the heat transfer correlations for SW and SR tubes, the $\overline{Nu}_{SW,SR}$ dependency on *Re* for each twist ratio examined can be revealed by plotting the developed flow heat transfer data against *Re*. As there is no significant change in the coolant Prandtl number (*Pr*) for the range of temperatures covered by the experimental program, the Prandtl number of coolant is treated as an invariant for the present study. It is assumed that the *Pr* impact on $\overline{Nu}_{SW,SR}$ follows the previous results reported by Hong and Bergles ($Pr = 3$–192) [3] and Agarwal and Rao ($Pr = 195$–375) [8] that $\overline{Nu}_{SW,SR} \propto Pr^{1/3}$. The present $\overline{Nu}_{SW,SR}$ data is accordingly normalized by $Pr^{1/3}$ for enhancing the generality of the heat transfer correlations derived by this study. Fig. 5 depicts the variations of $\overline{Nu}_{SW,SR}/Pr^{1/3}$ with *Re* for the SW and SR tubes. The simulated data using the correlation derived by Agarwal and Rao [8] is also displayed in Fig. 5 for validating the present results in the SW tube. The good agreement between the present SW tube re-

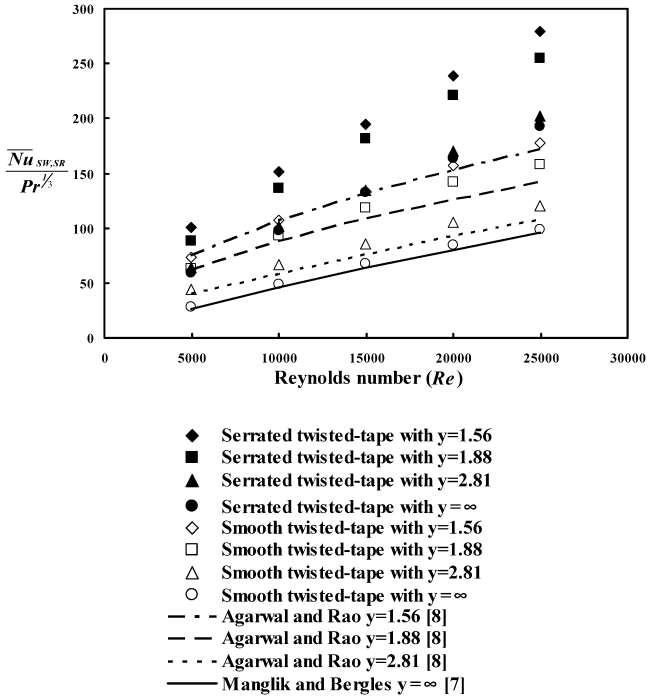

Fig. 5. Variations of normalized Nusselt number. $\overline{Nu}_{SW,SR}/Pr^{1/3}$ with Reynolds number in tubes fitted with twisted tape.

Table 1
Coefficients A and n in SW and SR tubes

$\overline{Nu}_{SW,RR} = A(y)Re^{n(y)}Pr^{1/3}$

y	SW tube		SR tube	
	A	n	A	n
1.56	0.696	0.547	0.454	0.633
1.88	0.457	0.578	0.309	0.663
2.81	0.218	0.623	0.148	0.711
∞	0.0364	0.782	0.118	0.73

sults and the correlative data of Agarwal and Rao [8] for three tested twist ratios are demonstrated in Fig. 5. It is noted that, with each twist ratio examined, the values of $\overline{Nu}_{SW,SR}/Pr^{1/3}$ for the SR tube increase at a faster rate with Re than its counterpart for the SW tube. Justified by each y controlled data series for either SW or SR tube as revealed in Fig. 5, the functional structure of $A(y) \times Re^{n(y)}$ is a suitable form to correlate all the data trends depicted in Fig. 5. Having the slight variation in Prandtl number of coolant been absorbed into the numerical coefficients of A and n, which are both functions of twist ratio (y), the Nusselt number correlations in the developed flow region of SW and SR tubes are generated. Table 1 summarizes the coefficients A and n derived for the SW and SR tubes with four twist ratios examined.

As listed in Table 1, the higher n value in the SR tube than that in the SW tube for each twist ratio tested indicates the stronger dependency of heat transfer on Re in the SR tube. This result has led to the increased effective Re range for HTE from the Dittus–Boelter condition [23] in the SR tube. The increase of n exponent with the increase of twist ratio in the SW and SR tubes suggests the extension of effective Re range for HTE as y increases. Fig. 6 plots the varying trends of coefficients A and n against Re. As depicted in Fig. 6, the coefficients A and n are exponentially decreased and increased respectively as y ratio increases. Having the $A(y)$ and $n(y)$ functions fitted with the exponential functions, the heat transfer correlations that permit the evaluation of $\overline{Nu}_{SW}$ and $\overline{Nu}_{SR}$ are derived in Eqs. (6) and (7), respectively.

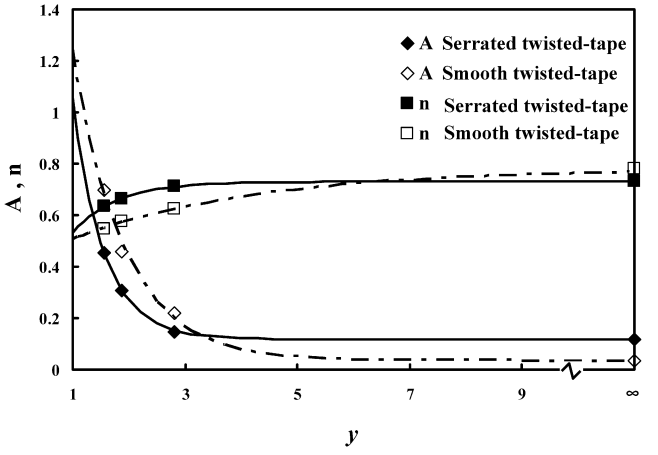

Fig. 6. Variations of coefficients A and n with Reynolds number for SW and SR tubes.

$$\overline{Nu}_{SW} = \left(0.0364 + 3.66e^{-1.11y}\right)Re^{(0.8-0.375e^{-0.31y})}Pr^{1/3} \quad (6)$$

$$\overline{Nu}_{SR} = \left(0.118 + 5.84e^{-1.83y}\right)Re^{(0.73-0.695e^{-1.26y})}Pr^{1/3} \quad (7)$$

Eqs. (6) and (7) predict the correlated data within ±8% that can be used to evaluate the heat transfer coefficients in the tubes fitted with SW or SR twisted tapes for the engineering design and retrofit applications.

3.2. Pressure drop results

Figs. 7 and 8 respectively display the axial distributions of the Fanning friction factor, f, in the SW and SR tubes with four twist ratios tested. With the finite twist ratio, the axial station where the f value is measured corresponds to the mid-pitch location of each twisted tape. As shown in Fig. 7, each Re controlled f-variation curve along the SW tube follows a general pattern of exponential decay in the streamwise direction. At each measured axial-location shown in Fig. 7, the f value consistently decreases with the increase of Re. However, the variation of f value with x/d and with Re in the SR tube tend to be reversed from those found in the SW tube. As depicted in Fig. 8 for the SR tube, the f vs. x/d relationship at each tested Re follows an exponential increase towards a constant developed flow value in the streamwise direction. The f value consistently increases with the increase of Re at each measured axial station in the SR tube. Nevertheless, the axial location corresponding to the developed flow region after which the f value remains constant is about 6 tube-diameters in both SW and SR tubes, which agrees with the result found from the heat transfer tests. The f values averaged from the developed flow region in each test tube are treated as the developed flow indicated by ($\bar{f}$). The pressure drop augmentation from the plain-tube level

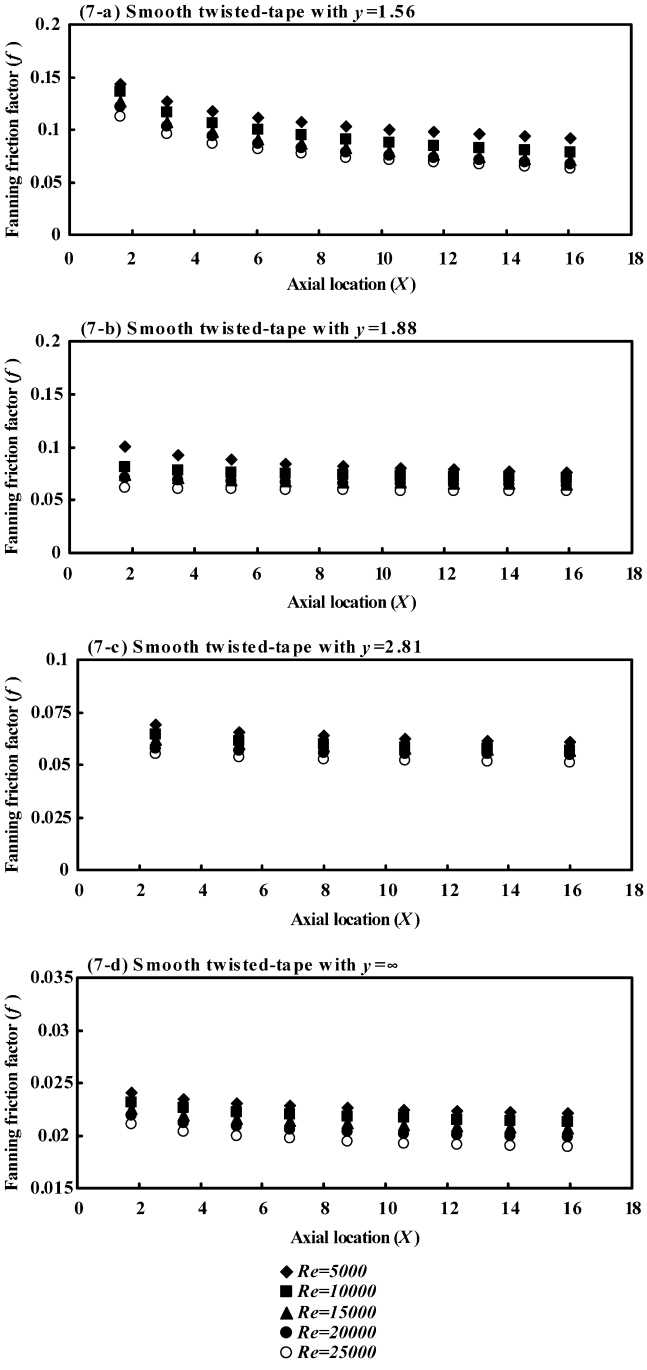

Fig. 7. Axial distributions of the Fanning friction factor in the SW tube.

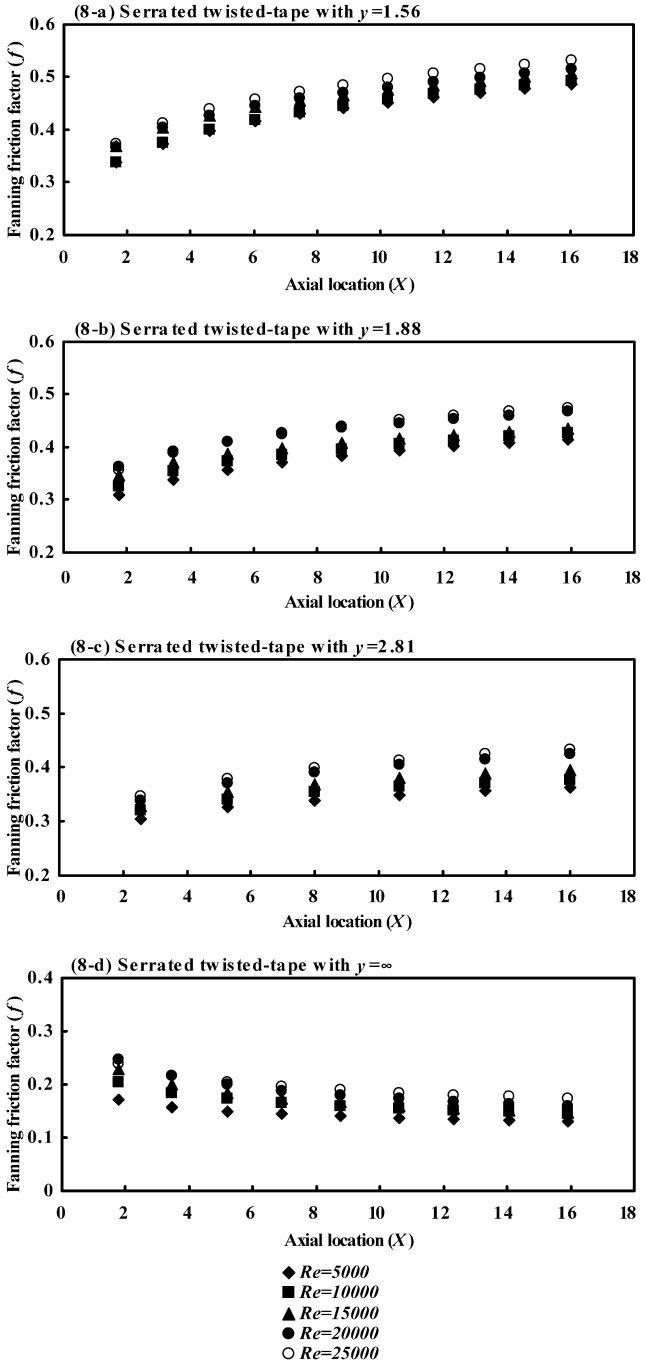

Fig. 8. Axial distributions of the Fanning friction factor in the SR tube.

due to the twisted tape insert is indexed as the relative f ratio in terms of $\bar{f}/f_\infty$ where the plain-tube level, f_∞, is evaluated from the Blasius equation. The variations of $\bar{f}$ value and $\bar{f}/f_\infty$ ratio against *Re* in the SW and SR tubes with three tested twist ratios are drawn in Figs. 9(a) and 9(b), respectively.

In Fig. 9(a), the calculated results using the $\overline{f}$ correlation reported by Manglik and Bergles [7] for the tube fitted with SW tube are also included in Fig. 9(a) to compare with the preset SW tube data for validation. The maximum discrepancy between the results of Manglik and Bergles [7] and the present SW tube data is in the range of ±15%. As shown in Fig. 9(a), the Fanning friction factors in the SW tube decrease with the increase of *Re* that tend to approach an asymptotic value as *Re* increases. In the SR tube as depicted in Fig. 9(a), each y controlled $\bar{f}$ variation also tends to approach an asymptotic value when *Re* increases but the $\bar{f}$ value increases with the increase of *Re* for four twist ratios tested. As shown in Fig. 9(a), the $\bar{f}$ value respectively decreases and increases with the increase of *Re* in the tubes fitted with smooth and serrated twisted tapes. In the smooth walled channel, it is common that the f factor decreases as *Re* increases. The flow physics for this particular f versus *Re* trend is usually explained using the concept of uni-

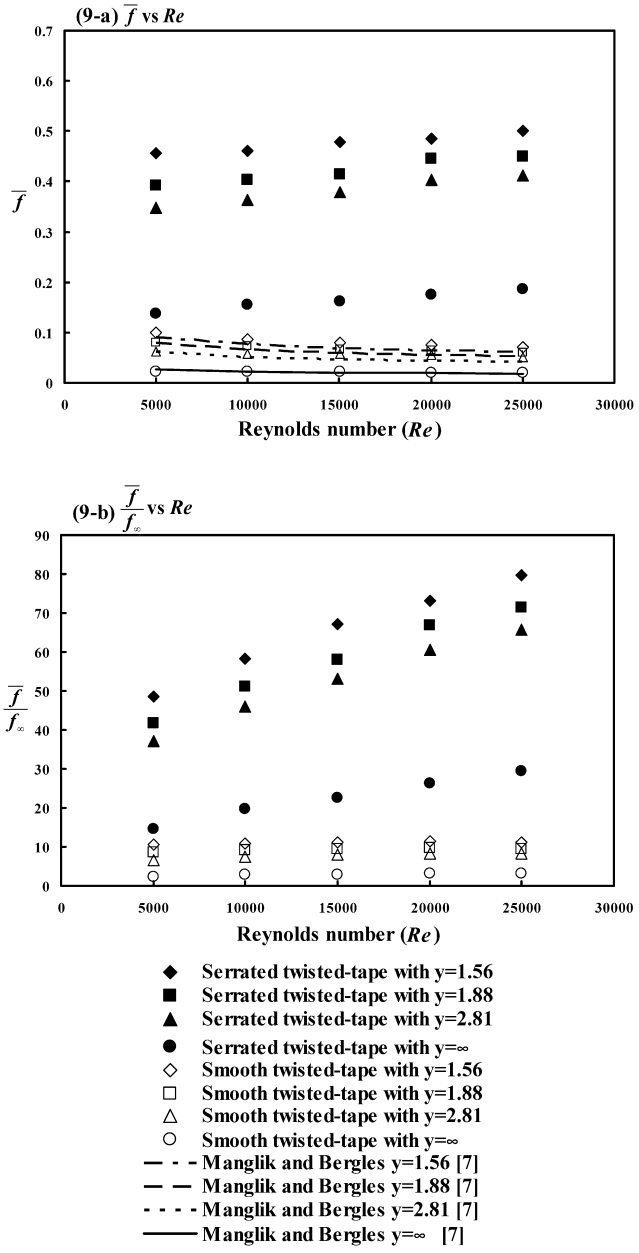

Fig. 9. Variations of $\bar{f}$ and $\bar{f}/f_\infty$ with Reynolds number.

versal wall function for turbulent pipe flow. The Prandtl mixing length theory has demonstrated that the thicknesses of buffer layer and sub-layer decrease as *Re* increases. As a result, the f factor is reduced due to the reduced thicknesses of the viscous layers as *Re* increases. However, in the rib roughened channel, the increase of *Re* enhances the turbulent shear stresses induced by the surface ribs. The shear layer on the boundary joining the vortical flow cells developed behind each rib and the main stream in the tube core considerably amplifies the turbulence intensity in this flow region. The turbulence intensity and the shear layer induce turbulence enhancement in the rib roughened channel increases as *Re* increases [25] so that the value in the rib roughened channel increases as *Re* increases. In the tube fitted with serrated twisted tape, the rib roughened twisted tape plays the role of a turbulator to enhance the turbulence intensity and induce the vortical flow cells behind each rib. As these surface ribs on the twisted tape follow the curvature of the tape with the inclination angle in respect to the main stream direction, the vortical flow cells behind these ribs are unlikely to be stagnant as those developed on the tape of $y = \infty$. Accompanying the swirling flows generated by the twisted tape, the vortical flow cells behind these surface ribs convect within the swirls in a dynamic manner to promote the vorticity. These interactive flow physics between the swirls and the rib induced vortices in the tube with serrated twisted tape provide the afore mentioned heat transfer augmentation with the penalty of increased value as *Re* increases. Furthermore, as the reference plain-tube f_∞ datum (Eq. (4)) decreases with the increase of *Re*, the data presentation in the manner of $\bar{f}/f_\infty$ vs. *Re* as revealed in Fig. 9(b) highlights the distinguishable difference between the SW and SR tubes. The friction ratios $\bar{f}/f_\infty$ decrease with the increase of *Re* in the SW tube but increase with the increase of *Re* in the SR tube. The reversing trend of $\overline{f}$ vs. *Re* relationship for the SR tube from the SW tube scenario could considerably determine the thermal performance of the SR tube at the high Reynolds numbers tested, which will be discussed in more detail when the thermal performance factors in the SW and SR tubes are compared. Based on the data trends revealed in Fig. 9(a), the $\overline{f}$ values in the SW and SR tubes are correlated into the functional structure of $B(y) \times Re^{m(y)}$ where the coefficients of B and m are both functions of twist ratio (y). In the present *Re* range of 5000–25 000, the correlations for the Fanning friction factor in the developed flow region of SW and SR tubes are generated. Table 2 summarizes the coefficients B and m derived for the SW and SR tubes with four twist ratios tested.

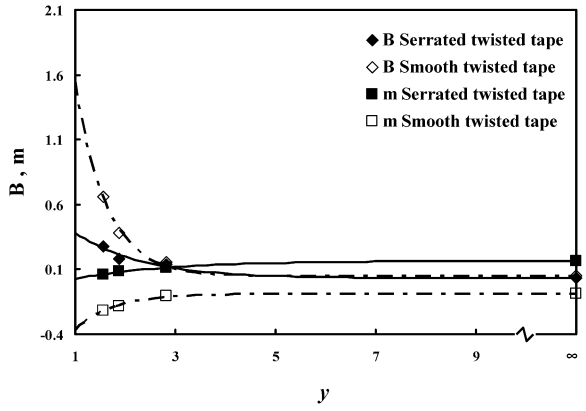

Fig. 10. Variations of coefficients B and m with Reynolds number. For SW and SR tubes.

Table 2
Coefficients B and m in SW and SR tubes

$\bar{f}_{SW,RR} = B(y)Re^{m(y)}$				
y	SW tube		SR tube	
	B	M	B	M
1.56	0.661	−0.214	0.280	0.056
1.88	0.382	−0.182	0.182	0.088
2.81	0.152	−0.103	0.137	0.108
∞	0.048	−0.088	0.033	0.166

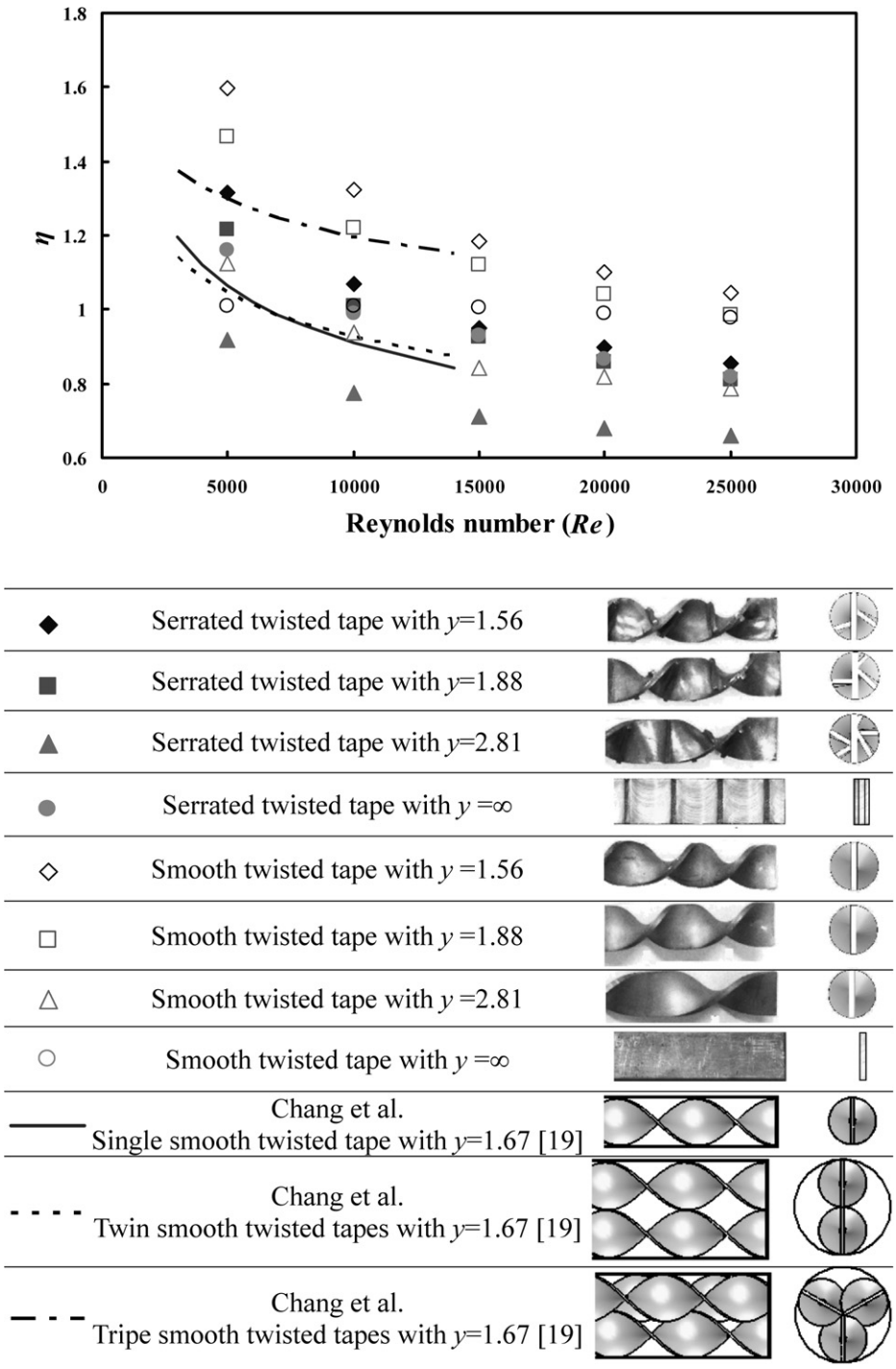

Fig. 11. Comparison of thermal performances in tubes fitted with twisted tapes.

Fig. 10 depicts the variation manners of coefficients B and m with Re. The coefficients B and m follow the exponential decay and increase as y ratio increases. With the $B(y)$ and $m(y)$ functions to be represented by the exponential functions, the Fanning friction factors in the SW and SR tubes are evaluated by Eqs. (8) and (9), respectively.

$$\bar{f}_{\mathrm{SW}} = \left(0.07 + 9.87e^{-1.81y}\right)Re^{(-0.08-0.94e^{-1.23y})} \tag{8}$$

$$\bar{f}_{\mathrm{SR}} = \left(0.033 + 0.756e^{-0.765y}\right)Re^{(0.166-0.235e^{-0.524y})} \tag{9}$$

Eqs. (8) and (9) provide the correlative results with maximum discrepancies of ±15% with the experimental measurements. The HTE ratio of $\overline{Nu}_{\mathrm{SW,SR}}/\overline{Nu}_{\infty}$ in the respective range of 1.59–3.5 and 2.66–4.8 times of the plain-tube level in the SW and SR tubes is accompanying with the increased pressure drop loss. Based on the same pumping power consumption, the thermal performance factor in terms of $(\overline{Nu}/Nu_{\infty})/(\bar{f}/f_{\infty})^{1/3}$ is compared between the SW and SR tubes with three twist ratios tested in Fig. 11. As shown in Fig. 11, with the same twist ratio, the SW tube consistently possesses the higher thermal perfor-

mance factor, η, than that of the SR tube. This particular result is derived from the increased $\bar{f}/f_\infty$ ratio as *Re* increases in the SR tube, even if the further HTE effect from the SW tube condition is obtained by using the SR twisted tape. In spite of the limiting conditions of $y = \infty$, the decrease of twist ratio in both SW and SR tubes increases the thermal performance factor in the present *Re* range of 5000–25 000. The thermal performance factors in the SR tube with twist ratios of 1.56 and 1.88 are higher than the η value in the SW tube with twist ratio of 2.81. Also included in Fig. 11 are the thermal performance factors in the tubes fitted with single, twin and triple smooth walled twisted tapes in the *Re* range of 3000–14 000 [19]. As compared in Fig. 11, the present test tube with the serrated twisted tape of 1.56, 1.87 or 2.81 y offers the similar levels of thermal performance factor as those found in the tubes fitted with twin and triple twisted tapes with twist-ratio of 2.81 y [19]. However, recalling the heat transfer performances compared in Fig. 5, the test tube fitted with rib roughened twisted tape offers the considerably higher value of HTE ratio than the counterpart in the SW tube. The SR tube is considered as an effective mean for further heat transfer augmentation from the SW tube level that is subject to a reasonable reduction in the thermal performance factor.

4. Conclusions

A comparative study of heat transfer and pressure drop in the tubes fitted with the smooth walled and serrated twisted tapes with twist ratios of 1.56, 1.88, 2.81 and ∞ has been carried out in the *Re* range of 5000–25 000. Accompanied by a reduction of thermal performance factor, the tube with serrated twisted tape insert is an effective measure for further heat transfer augmentation from the level in the tube fitted with smooth walled twisted tape. Several salient concluding remarks are revealed by the present study, which are summarized as follows:

(1) The increase of *Re* or twist ratio (y) in either SW or SR tube reduces the $\overline{Nu}_{SW,SR}/\overline{Nu}_\infty$ ratio. In the *Re* range of 5000–25 000, the $\overline{Nu}_{SW,SR}/\overline{Nu}_\infty$ ratios obtained with four tested twist ratios are in the ranges of 3.5–2.34, 2.99–2.07, 2.12–1.59 and 1.35–1.31 for the SW tube and in the ranges of 4.8–3.68, 4.21–3.36, 3.06–2.66 and 2.84–2.53 for the SR tube.

(2) The relative heat transfer enhancements in the SR tube from the SW tube level for three twist ratios tested fall in the range of 1.25–1.67 times of $\overline{Nu}_{SW}$ value in the *Re* range of 5000–25 000. The relative Nusselt number of $\overline{Nu}_{SR}/\overline{Nu}_{SW}$ increases with the increase of *Re* for the finite twist ratios tested so that the HTE effectiveness with serrated twisted tape is enhanced as *Re* increases. As a result, the SR tube can extend the effective *Re* range for HTE from the SW tube condition.

(3) In the SW tube, the axial variation of f value follows a general pattern of exponential decay toward a fully developed level with the local f value to be decreased with the increase of *Re*. In the SR tube, the variations of f vs. x/d and *Re* are reversed from those found in the SW tube. The axial variation of f value follows an exponential increase toward a constant developed flow value with the local f value to be increased with the increase of *Re* in the SR tube.

(4) The $\bar{f}$ values in the SW tube decrease with the increase of *Re* following a tendency of approaching the asymptotic value. In the SR tube, the varying manner of $\bar{f}$ with *Re* also tends to approach toward an asymptotic value as *Re* increases but the $\bar{f}$ value increases with the increase of *Re*. In both SW and SR tubes, the $\bar{f}$ values consistently increase with the decrease of twist ratio.

(5) With the same twist ratio, the SW tube consistently provides the higher thermal performance factor, η, than its counterpart of SR tube. In the present *Re* range tested, the decrease of twist ratio in both SW and SR tubes increases the thermal performance factor.

(6) One set of heat transfer and pressure drop correlations that evaluate the Nusselt number and the Fanning friction factor of developed flow in the tubes fitted with smooth and serrated twisted tapes with four twist ratios of 1.56, 1.88, 2.81 and ∞ are generated.

References

[1] S. Martemianov, V.L. Okulov, On heat transfer enhancement in swirl pipe flows, Int. J. Heat Mass Transfer 47 (2004) 2379–2393.

[2] E. Smithberg, F. Landies, Friction and forced convection heat transfer characteristics in tubes with twisted tape swirl generators, ASME J. Heat Transfer 86 (1964) 39–49.

[3] S.W. Hong, A.E. Bergles, Augmentation of laminar flow heat transfer in tubes by means of twisted tape inserts, ASME J. Heat Transfer 98 (1976) 251–256.

[4] R.M. Manglik, A.E. Bergles, Laminar flow heat transfer in a semi-circular tube with uniform wall temperature, Int. J. Heat Mass Transfer 31 (3) (1988) 625–636.

[5] W.J. Marner, A.E. Bergles, J.M. Chenoweth, On the presentation of performance data for enhanced tubes used in shell-and-tube heat exchangers, ASME J. Heat Transfer 105 (1983) 358–365.

[6] R.M. Manglik, A.E. Bergles, Heat transfer and pressure drop correlations for twisted tape inserts in isothermal tubes: Part I – Laminar flows, ASME J. Heat Transfer 115 (1993) 881–889.

[7] R.M. Manglik, A.E. Bergles, Heat transfer and pressure drop correlations for twisted tape inserts in isothermal tubes: Part II – Transition and turbulent flows, ASME J. Heat Transfer 115 (1993) 890–896.

[8] S.K. Agarwal, R.M. Raja, Heat transfer augmentation for the flow of a viscous liquid in circular tubes using twisted tape inserts, Int. J. Heat Mass Transfer 39 (17) (1996) 3547–3557.

[9] S.W. Chang, Heat transfer of orthogonal-mode reciprocating tube fitted with twisted tape, J. Experimental Heat Transfer 13 (2000) 61–86.

[10] S.W. Chang, Heat transfer of parallel-mode reciprocating tube flow with twisted tape insert for piston cooling application, ASME J. Gas Turbine Power 123 (2001) 146–156.

[11] L. Wang, B. Sundén, Performance comparison of some tube inserts, Int. Comm. Heat Mass Transfer 29 (1) (2002) 45–56.

[12] P.K. Sarma, P.S. Kishore, V.R. Dharma, T. Subrahmanyam, A combined approach to predict friction coefficients and convective heat transfer characteristics in a tube with twisted tape inserts for a wide range of *Re* and *Pr*, Int. J. Thermal Sci. 44 (2005) 393–398.

[13] S.K. Saha, U.N. Gaitonde, A.W. Date, Heat transfer and pressure drop characteristics of laminar flow in a circular tube fitted with regularly spaced twisted tape elements, Exp. Therm. Fluid Sci. 2 (3) (1989) 310–322.

[14] S.K. Saha, A. Dutta, S.K. Dhal, Friction and heat transfer characteristics of laminar swirl flow through a circular tube fitted with regularly spaced twisted tape elements, Int. J. Heat Mass Transfer 44 (2001) 4211–4223.
[15] V. Zimparov, Enhancement of heat transfer by a combination of three-start spirally corrugated tubes with a twisted tape, Int. J. Heat Mass Transfer 44 (2001) 551–574.
[16] V. Zimparov, Enhancement of heat transfer by a combination of a single start spirally corrugated tubes with a twisted tape, Exp. Thermal Fluid Science 25 (2002) 535–546.
[17] S. Ray, A.W. Date, Laminar flow and heat transfer through square duct with twisted tape insert, Int. J. Heat Fluid Flow 22 (2001) 460–472.
[18] S.W. Chang, Y. Zheng, Enhanced heat transfer with swirl duct under rolling and pitching environment, J. Ship Research 46 (2002) 149–166.
[19] S.W. Chang, K.W. Yu, M.H. Lu, Heat transfer in tubes fitted with single, twin and triple twisted tapes, J. Experimental Heat Transfer 18 (2005) 279–294.
[20] S.W. Chang, Y.J. Jan, L.M. Su, Heat transfer in an axially rotating tube fitted with twin twisted tapes, JSME Int. J. B. Fluids and Thermal Engrg. 47 (2004) 637–646.
[21] A.E. Bergles, ExHFT for fourth generation heat transfer technology, Experimental Thermal Fluid Sci. 26 (2002) 335–344.
[22] D. Neshumayev, A. Ots, J. Laid, T. Tiikma, Experimental investigation of various turbulator inserts in gas-heated channels, Experimental Thermal Fluid Sci. 28 (2004) 877–886.
[23] F.W. Dittus, L.M.K. Boelter, University of California, Berkeley, CA, Publications in Engineering, vol. 2, 1930, p. 443.
[24] Editorial Board of ASME Journal of Heat Transfer, Journal of heat transfer policy on reporting uncertainties in experimental measurements and results, ASME J. Heat Transfer 115 (1993) 5–6.
[25] H. Sato, K. Hishida, M. Maeda, Characteristics of turbulent flow and heat transfer in a rectangular channel with repeated rib roughness, Experimental Heat Transfer 5 (1992) 1–16.